Defect-Enhanced Charge Transfer by Ion-Solid Interactions in SiC using Large-Scale *Ab Initio* Molecular Dynamics Simulations

Fei Gao,[1] Haiyan Xiao,[2] Xiaotao Zu,[2] Matthias Posselt,[3] and William J. Weber[1]

[1]*Pacific Northwest National Laboratory, P. O. Box 999, Richland, Washington 99352, USA*

[2]*Department of Applied Physics, University of Electronic Science and Technology of China, Chengdu, 610054, China*

[3]*Forschungszentrum Dresden-Rossendorf, Institute of Ion Beam Physics and Materials Research, D-01314 Dresden, Germany*

(Received 31 July 2008; published 10 July 2009)

Large-scale *ab initio* molecular dynamics simulations of ion-solid interactions in SiC reveal that significant charge transfer occurs between atoms, and defects can enhance charge transfer to surrounding atoms. The results demonstrate that charge transfer to and from recoiling atoms can alter the energy barriers and dynamics for stable defect formation. The present simulations illustrate in detail the dynamic processes for charged defect formation. The averaged values of displacement threshold energies along four main crystallographic directions are smaller than those determined by empirical potentials due to charge-transfer effects on recoil atoms.

DOI: 10.1103/PhysRevLett.103.027405 PACS numbers: 78.70.−g, 31.15.ae, 34.70.+e, 82.30.Fi

The interaction of energetic ions with solids can lead to the modification of mechanical, magnetic, electrical, and optical properties of materials. Defect creation and damage accumulation from ion-solid interactions are also important to space and nuclear applications. Understanding the basics of ion-solid interactions has led to significant developments in state-of-the-art molecular dynamics (MD) simulations with empirical potentials, and these simulations have dramatically advanced the understanding of defects and defect processes in a number of metals [1], semiconductors [2], and oxides [3]. However, these classical MD approaches do not provide information on the response in the electronic structure from ion-solid interactions, which represents a computational challenge beyond classical MD simulations.

Simultaneous electronic and atomic collisions can change the charge state of existing and newly created defects [4], affecting both defect creation and clustering. Defect diffusion mechanisms and corresponding migration energies also depend strongly on defect charge states, particularly in covalent and ionic materials [5,6]. It has been shown that the charge state of preexisting interstitials can be changed under low-energy electron irradiation, leading to radiation-enhanced annealing that has been observed in Si, Ge, diamond, and GaAs [7–10]. Although radiation-enhanced annealing is a well-known process in the physics and materials communities, the theoretical interpretation remains controversial [11,12]. Furthermore, the dynamic process of charge transfer can produce competing effects in semiconductors and ceramics. A framework for modeling these effects, based on defect production and defect annealing, has been considered over the past decade [13], but detailed simulations have not yet been performed.

Here we employ large-scale *ab initio* molecular dynamics to investigate defect formation from low-energy recoil events in 3*C*-SiC [14]. By considering atomic dynamics and electronic structure effects on defect generation, charge transfer and charge-density redistribution are directly observed, and defect creation is found to be affected by charge-transfer processes. SiC was chosen for this initial study because it represents a well-understood model system for two-component covalent materials. Furthermore, SiC is of great interest because it has significant potential for technological applications in nuclear environments [15] and high temperature optoelectronic devices [16].

Ab initio molecular dynamics simulations were performed using the SIESTA code [17], based on density functional theory within the framework of the local density approximation. The exchange-correlation potential proposed by Ceperley-Alder and parametrized by Perdew and Zunger [18] was used. Troullier-Martins pseudopotentials were used to take into account the effect of core electrons [19]. Simulations of recoil events were performed in a 1000-atom supercell ($5a_0 \times 5a_0 \times 5a_0$) with Γ-point sampling in the Brillouin zone, single-ζ basis sets, and a 90 Ry cutoff for the real space mesh. The convergence of our calculations has been tested, and errors up to 2 eV in threshold displacement energy (E_d) are expected, as compared with those using double-ζ basis sets plus polarization orbitals. To simulate ion-solid interactions, the SIESTA code has been modified to initiate the primary knock-on atom (PKA) with kinetic energy (KE) in a given direction and to include a variable time step (0.001–1 fs) approach [20]. To determine the final defect configurations and the energy barriers for defect formation, the relaxation of the corresponding atomic configurations was carried out with a $2 \times 2 \times 2$ k-point sampling and double-ζ basis sets plus polarization orbitals. With these parameters, the calculated lattice parameter $a_0 = 4.36$ Å and the bulk modulus $B = 226$ GPa were found to be in good agreement with the experimental values of 4.36 Å and 224 GPa [21], respectively. The formation energies of intrinsic defects

and defect configurations are also in good agreement with previous theoretical calculations [22]. A Nosé-Hoover thermostat was applied to the boundary atoms in both the equilibrating stage of the crystal and the energy recoil stage. With this approach, an equilibrium state can be achieved within 0.5 ps at 100 K. Periodic boundary conditions were applied along three directions. The supercell was equilibrated at 100 K for a much longer time (~5 ps) than the time constant of the N-H thermostat to make sure that the system was well equilibrated before the PKA event was initiated. The atoms were then allowed to evolve for about 2 ps after the PKA was initiated. Four high symmetry directions ([100], [110], [111], and $[\bar{1}\,\bar{1}\,\bar{1}]$ directions) for both Si and C sublattices are considered, with four different simulations for each direction. The results show no significant differences in the trajectories, charge variation of the PKA, and stable defect formation for these low-energy recoils. In order to clearly present the physics involved, only the dynamic processes for the C and Si recoil events along the $[\bar{1}\,\bar{1}\,\bar{1}]$ direction are discussed in detail, but general conclusions can be applied to C and Si recoils along other directions.

The atomic configurations in Fig. 1(a) show three stages in a typical process of defect formation, after a kinetic energy of 62 eV is transferred to a Si PKA along the $[\bar{1}\,\bar{1}\,\bar{1}]$ direction. For a recoil event of 60 eV, the Si PKA passes through an initial energy window (the first tetrahedral position) consisting of four C atoms, as indicated by the first gray sphere in configuration (A), and fails to pass the second energy window, resulting in the PKA atom recoiling to its original position. If the kinetic energy is above E_d (62 eV), the PKA passes the two energy windows and directly interacts with a C atom. This process transfers sufficient energy to the C atom to create a short replacement collision sequence involving two Si and one C atoms, as shown in configuration (B). A strong back recoil results in the Si and C atoms returning to their lattice sites, and the initially struck C atom pushes the Si PKA atom slightly off the $[\bar{1}\,\bar{1}\,\bar{1}]$ direction, forming a Si tetrahedral interstitial surrounding by four C atoms (Si_{TC}), as shown in configuration (C).

The charge-density difference $\Delta\rho$ in the $(1\bar{1}0)$ plane that contains the Si PKA is investigated. The charge-density contour plot for the final configuration (C) is provided in Fig. 1(b). The Si tetrahedral interstitial (PKA) forms new bonds with its nearest C atoms, as shown by the charge accumulation in the bonding regions. Upon closer inspection, the distances between the Si_{TC} and its two second-nearest Si atoms in this plane are found to be approximately the same, i.e., 2.59 and 2.56 Å for the one above the Si_{TC} and the one below, respectively. However, the Si_{TC} prefers to form a new bond with the Si atom below (indicated by an arrow). A strong bond formed between the Si_{TC} and its nearest C atom may facilitate the charge transfer between the two nearby Si atoms, leading to charge accumulation in the bonded regions and the formation of a new covalent bond. Figure 1(b) also clearly shows that the Si vacancy does not pair with its neighboring atoms, and the Si vacancy is in a negatively charged state (relative to a Si atom in 3*C*-SiC).

To elucidate the role of charge transfer and charge redistribution on defect dynamics, we have carried out a detailed analysis of the charge variation of a C PKA. Figure 2 shows the variation of the calculated Mulliken charges on the C PKA during a C recoil event of 47.5 eV along the $[\bar{1}\,\bar{1}\,\bar{1}]$ direction. Bader charge analysis was also performed in perfect SiC using the program developed by Henkelman, Arnaldsson, and Jónsson [23], and the calculated effective charges for C and Si atoms are 4.523 and 3.477$|e|$, respectively, in reasonable agreement with the Mulliken charges of 4.764 and 3.236$|e|$ and the values of 4.887 and 3.113 obtained using the *ab initio* orthogonalized linear combination of the atomic orbital method [24]. The

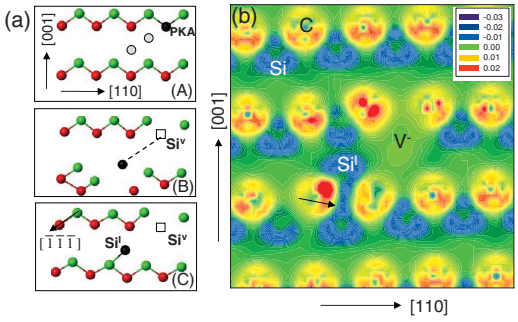

FIG. 1 (color). (a) Three atomic configurations in a $(1\bar{1}0)$ plane showing defect generation at times of (A) 0.55, (B) 1.02, and (C) 2.0 ps, where the red and green spheres are Si and C atoms, respectively, and the Si PKA is represented by a black sphere and the Si vacancy by a white square. The gray spheres indicate two tetrahedral positions. (b) Charge-density difference contour plot for the final atomic configuration (C) in a $(1\bar{1}0)$ plane in units of $|e|/a_b{}^3$ (a_b-Bohr radius).

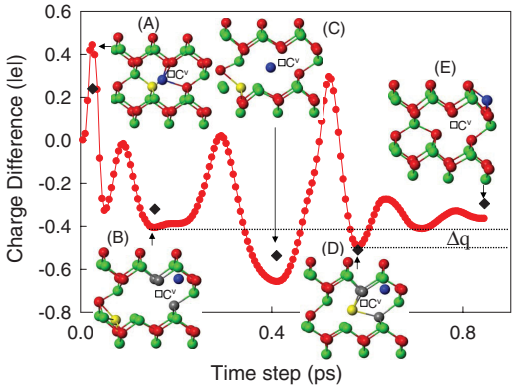

FIG. 2 (color). Variation of effective charge, gain (+), and loss (−) of electrons, for the C PKA along the $[\bar{1}\,\bar{1}\,\bar{1}]$ direction, where the orientations of the atomic configurations are the same as those in Fig. 1. The blue and yellow spheres represent the C PKA and secondary Si recoil atom, respectively, and the black diamonds indicate the charge differences obtained from the Bader charge analysis.

charge differences obtained by Bader charge analysis for several atomic configurations are included in Fig. 2 and show a similar tendency. The charge is relative to the effective charge of a C atom in perfect 3*C*-SiC. Atomic configuration (A) in Fig. 2 shows that the C PKA initially moves along the $[\bar{1}\,\bar{1}\,\bar{1}]$ direction and then directly interacts with a Si atom [shown as a yellow sphere and denoted as the secondary recoil atom (SRA)]. The SRA transfers charge during this process, with a maximum charge transfer of about $0.442|e|$ to the C PKA and $0.127|e|$ to the SRA's nearest-neighbor C atoms. Although most charge from the SRA is transferred to the C PKA, the present results demonstrate that a defect can enhance charge transfer to surrounding atoms. At this stage, the strong repulsive interaction between the PKA and SRA forces the SRA to move along the $[\bar{1}\,\bar{1}\,\bar{1}]$ direction, but the PKA rebounds and moves in the opposite [111] direction. Atomic configuration (B) shows a metastable state, where the PKA is in a tetrahedral position. The C PKA transfers a charge of $0.41|e|$ to three Si atoms (as indicated by the gray spheres) that are the nearest neighbors to the vacancy. The C PKA stays in this position for a number of time steps, as shown by a plateau in Fig. 2, but fails in overcoming the energy barrier to form a stable interstitial. Consequently, the C PKA rebounds back along the original $[\bar{1}\,\bar{1}\,\bar{1}]$ direction and gains charge from three nearby Si atoms. The PKA passes through its original position and interacts with the Si SRA again, as indicated by configuration (C). In this process, the C PKA loses charge to the same three Si atoms, and the nearest-neighbor C atoms to the three Si atoms also transfer charge to these Si atoms. However, the striking feature is that the C PKA transfers $0.42|e|$ to the SRA even though the distance between them is about 3 Å. The interaction between the PKA and the SRA once again reverses the PKA's direction and forces it to move along the [111] direction. The SRA returns to its original position during this process, while the C PKA continuously propagates along the same direction and eventually passes a window consisting of four C atoms, as shown in configuration (D). This process leads to the formation of a C interstitial in a tetrahedral position surrounding by four Si atoms, as illustrated in configuration (E). Further simulation transforms the C tetrahedral defect into a C-C$\langle 100 \rangle$ split interstitial that is the most stable configuration for C interstitials in SiC [25]. In configuration (D), the charge gain of the three Si atoms is similar to that in configuration (B), but the C PKA also transfers some of the charge to the remaining Si neighbor atoms. The difference in the charge states of the C PKA between configurations (B) and (D), as shown in Fig. 2, is about 0.11 electrons, with more negative charge in configuration (D). This charge difference may lower the energy barrier the C PKA passes to form a stable Frenkel pair.

A series of atomic configurations has been minimized using the conjugate gradient method to calculate the energy variation with high precision. The calculated results are shown in Fig. 3, where the energy is relative to the total energy of perfect SiC. The energy barrier for the C PKA to pass the window in atomic configuration (D) is about 3.2 eV lower than that in configuration (B). This clearly illustrates that the lower charge state of the C PKA in atomic configuration (D) decreases the energy barrier, which may provide an explanation as to why the C PKA does not pass the energy window the first time [configuration (B)] but does pass the second time. The dynamic evolution for this C PKA is clearly a charge-transfer-assisted process leading to stable defect formation.

Similar to the Si PKA event, charge-density contour plots for atomic configurations (B), (D), and (E) in Fig. 2 are provided in Figs. 4(a)–4(c), respectively. In Fig. 4(a), the C PKA transfers charge to one of its nearest Si neighbors, as indicated by the arrow, but the SRA Si atom prefers to form a bond with its nearest Si neighbor, as the charge begins to accumulate in the bonding regions. One of the C atoms above also transfers some charge to the nonbonding regions, forming directional bonds with its neighbor atoms, with either Si or C atoms. This striking profile is indicative of defect-enhanced change transfer. In Fig. 4(b), the most interesting observation is that some charge accumulates on the C vacancy, mainly transferred from the C PKA. The charge is mostly distributed in the region between the C vacancy and its two Si neighbor atoms, suggesting a tendency for pairing of two Si atoms neighboring the C vacancy. As soon as the C PKA passes the energy barrier, further charge transfer from the surrounding atoms to the C vacancy occurs, as indicated by the arrow in Fig. 4(c). Obviously, this C vacancy is a positively charged vacancy (relative to a C atom in 3*C*-SiC). Two neighboring Si atoms of the C vacancy in a plane parallel to one of the (100) planes move towards each other, forming a dimerlike bond with a length of 2.78 Å, while the other two are stretched in a plane parallel to one of the (001) planes with a separation of 3.23 Å. These results indicate the pairing mechanism for Si atoms neighboring the C vacancy, reducing the ideal T_d symmetry to a local tetragonal D_{2d} symmetry, which represents a significant Jahn-Teller distortion. It is also ob-

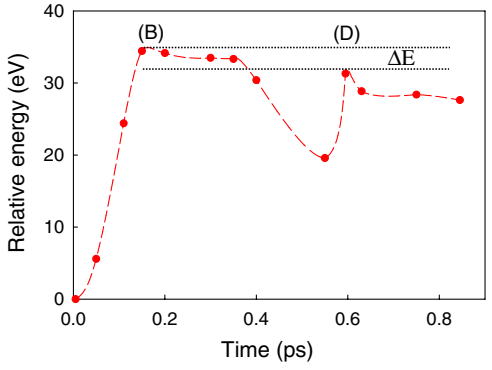

FIG. 3 (color online). Variation of relative energy of the system as a function of time step, where there are two energy barriers corresponding to atomic configurations (B) and (D), respectively.

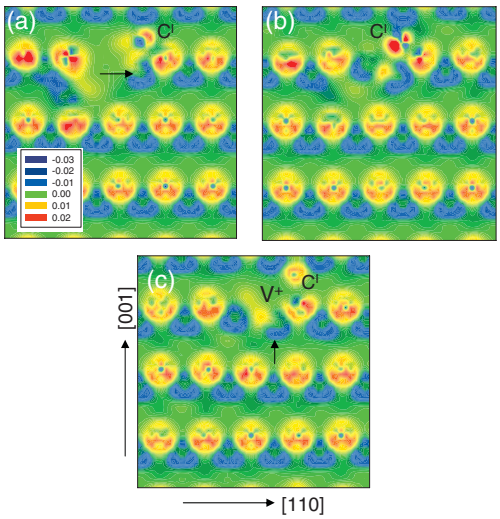

FIG. 4 (color). Charge-density contours (a), (b), and (c) in a $(1\bar{1}0)$ plane for atomic configurations (B), (D), and (E) in Fig. 2, respectively, where the vacancy and C interstitial are indicated.

served that the accumulated charge is not in the center of the vacancy, and the strong interaction of the charged vacancy with neighbors leads to this distortion. Experimentally, the carbon vacancy has been previously identified by electron paramagnetic resonance as a positively charged vacancy in proton-irradiated 3*C*-SiC [26] and electron-irradiated 4*H*- and 6*H*-SiC [27], consistent with these results.

The E_d for C and Si atoms along the $[\bar{1}\,\bar{1}\,\bar{1}]$ direction are determined to be 47.5 and 62 eV, respectively. The weighted average E_d values for the four main crystallographic directions are about 25.5 eV for C and 46.2 eV for Si. These values are smaller than the weighted values for the same directions determined using Tersoff potential MD calculations [28] (41 and 63 eV for C and Si recoils, respectively), and this may be due to the fact that the PKAs generally transfer their charge to the surrounding atoms, which alters the energy barriers for the formation of stable Frenkel pairs, as discussed above.

In conclusion, *ab initio* MD simulations have been employed to study ion-solid interactions, to explore defect-enhanced charge transfer and charge-density redistribution, and to understand the dynamic processes of charge defect formation. The charge variation of recoil atoms can alter the energy barrier for stable defect formation, and the corresponding dynamic evolution is a charge-transfer-assisted process. In addition, the defects formed during recoil events can enhance charge transfer to surrounding atoms, and this affects charge-density redistribution. The simulations also provide important insights into the formation of charged vacancy defects. The C vacancy is a positively charged defect that exhibits a significant Jahn-Teller distortion, whereas the Si vacancy is a negatively charged defect.

This research is supported by the Division of Materials Sciences and Engineering, Office of Basic Energy Sciences, U.S. Department of Energy under Contract No. DE-AC05-76RL01830. We thank Professor Marshall Stoneham for helpful suggestions regarding the manuscript.

[1] D. J. Bacon, F. Gao, and Yu. N. Osetsky, J. Nucl. Mater. **276**, 1 (2000).
[2] F. Gao and W. J. Weber, Phys. Rev. B **66**, 024106 (2002).
[3] A. Chartier, C. Meis, J.-P. Crocombette, W. J. Weber, and L. R. Corrales, Phys. Rev. Lett. **94**, 025505 (2005).
[4] M. Y. Fan, in *Radiation Effects in Semiconductors*, edited by J. W. Corbett and G. D. Watkins (Gordon and Breach, New York, 1971), p. 293.
[5] M. J. Beck, L. Tsetseris, and S. T. Pantelides, Phys. Rev. Lett. **99**, 215503 (2007).
[6] A. M. Stoneham and M. J. L. Sangster, Philos. Mag. B **52**, 717 (1985).
[7] K. Thommen, Radiat. Eff. **2**, 201 (1970).
[8] J. W. MacKay, E. E. Klontz, and G. W. Gobeli, Phys. Rev. Lett. **2**, 146 (1959).
[9] L. L. Sivo and E. E. Klontz, Phys. Rev. **178**, 1264 (1969).
[10] D. J. Twitchen *et al.*, Physica (Amsterdam) **273B–274B**, 644 (1999).
[11] S. J. Zinkle, V. A. Skuratov, and D. T. Hoelzer, Nucl. Instrum. Methods Phys. Res., Sect. B **191**, 758 (2002).
[12] W. J. Weber, L. Wang, Y. Zhang, W. Jiang, and I.-T. Bae, Nucl. Instrum. Methods Phys. Res., Sect. B **266**, 2793 (2008).
[13] W. J. Weber, R. C. Ewing, C. R. A. Catlow, T. Diaz de la Rubia, L. W. Hobbs, C. Kinoshita, H. Matzke, A. T. Motta, M. Nastasi, E. K. H. Saljie, E. R. Vance, and S. J. Zinkle, J. Mater. Res. **13**, 1434 (1998).
[14] M. Posselt, F. Gao, and W. J. Weber, Phys. Rev. B **73**, 125206 (2006).
[15] A. Azzam Yasseen, Chien Hung Wu, C. A. Zorman, and M. Mehregany, IEEE Electron Device Lett. **21**, 164 (2000).
[16] P. Mélinon, B. Mashnelli, F. Tournus, and A. Perez, Nature Mater. **6**, 479 (2007).
[17] J. M. Soler *et al.*, J. Phys. Condens. Matter **14**, 2745 (2002).
[18] J. P. Perdew and A. Zunger, Phys. Rev. B **23**, 5048 (1981).
[19] N. Troullier and J. L. Martins, Phys. Rev. B **43**, 1993 (1991).
[20] A. J. E. Foreman, C. A. English, and W. J. Phythian, Philos. Mag. A **66**, 655 (1992).
[21] D. H. Yean and J. R. Riter, Jr., J. Phys. Chem. Solids **32**, 653 (1971).
[22] F. Gao, W. J. Weber, H. Y. Xiao, and X. T. Zu, Nucl. Instrum. Methods Phys. Res., Sect. B (to be published).
[23] G. Henkelman, A. Arnaldsson, and H. Jónsson, Comput. Mater. Sci. **36**, 354 (2006).
[24] P. Rulis, W. Y. Ching, and M. Kohyama, Acta Mater. **52**, 3009 (2004).
[25] F. Gao, E. J. Bylaska, W. J. Weber, and L. R. Corrales, Phys. Rev. B **64**, 245208 (2001).
[26] H. Itoh, M. Yoshikawa, I. Nashiyama, S. Misawa, H. Okumura, and S. Yoshida, J. Electron. Mater. **21**, 707 (1992).
[27] N. T. Son, P. N. Hai, and E. Janzén, Phys. Rev. B **63**, 201201 (2001).
[28] R. Devanathan, T. Diaz de la Rubia, and W. J. Weber, J. Nucl. Mater. **253**, 47 (1998).